

Surface and foam properties of SLES + CAPB + fatty acid mixtures: Effect of pH for C12–C16 acids

Z. Mitrinova^a, S. Tcholakova^{a,*}, K. Golemanov^a, N. Denkov^a, M. Vethamuthu^b, K.P. Ananthapadmanabhan^b

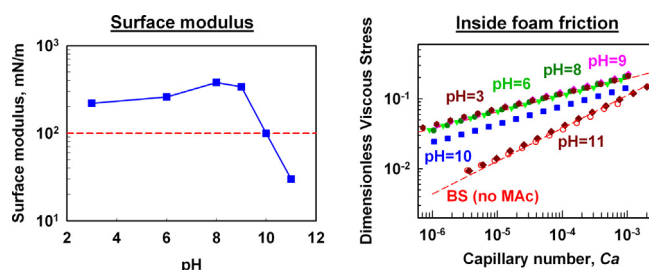
^a Department of Chemical Engineering, Faculty of Chemistry and Pharmacy, Sofia University, 1 J. Bourchier Ave., 1164 Sofia, Bulgaria

^b Unilever Global Research Center, Trumbull, CT 06611, USA

HIGHLIGHTS

- ▶ Effects of pH and fatty acid chain length on foam and surface properties is studied.
- ▶ Increase of pH above a threshold value leads to sharp decrease of surface modulus.
- ▶ Decrease of surface modulus below 100 mN/m leads to jump in foam properties.
- ▶ Threshold pH value increases from 8 to 11 with the increase of acid chain length

GRAPHICAL ABSTRACT



ARTICLE INFO

Article history:

Received 28 August 2012

Received in revised form 7 December 2012

Accepted 8 December 2012

Available online 20 December 2012

Keywords:

Surface dilatational modulus

Fatty acid chain length

Cosurfactant

Foam rheology

Foam-wall friction

ABSTRACT

Recently we showed that triple surfactant mixtures, comprising the anionic surfactant SLES, zwitterionic surfactant CAPB and long-chain fatty acid (FAC), possess very high surface modulus which can be used to modify the dynamic properties of foams (Golemanov et al. Langmuir 2008, 24, 9956). In the current paper we perform a systematic experimental study of the effects of several factors on the surface tension, surface dilatational modulus, viscous friction inside sheared foam, foam-wall friction, and mean bubble size in sheared foams, for such triple surfactant mixtures. The factors studied are: (1) chain length of fatty acid; (2) fatty acid concentration; (3) pH; (4) presence of glycerol in the aqueous solution. Lauric (C12Ac), myristic (C14Ac) and palmitic (C16Ac) acids are studied. The concentrations of the main surfactants were fixed, 10 mM for SLES and 5 mM for CAPB. Varying the myristic acid (C14Ac) concentration, C_{C14Ac} , we observed two ranges: (1) At $C_{C14Ac} < 0.06$ mM, the acid increases the solution surface modulus up to 50 mN/m, however, without affecting significantly any of the other properties studied; (2) At $C_{C14Ac} > 0.11$ mM, C14Ac leads to significant decrease of surface tension (from 29 to 22 mN/m), increase of surface modulus (from 50 to 400 mN/m), decrease of mean bubble size in sheared foams (from 300 to 150 μ m), and strong increase of the inside-foam friction and foam-wall friction. Qualitatively similar results are obtained with the other FAC studied. Mass-balance estimates show that low surface tension and high surface modulus are observed, when the molar fraction of FAC in the adsorption layer approaches ca. 30%. The main role of FAC is to induce a surface phase transition, leading to formation of surface condensed phase in the mixed adsorption layer. For all systems studied, the increase of pH above a certain transitional value leads to a sharp increase of surface tension and decrease of surface dilatational modulus, which is accompanied with a decrease in the inside-foam and foam-wall viscous

Abbreviations: BS, mixture of SLES and CAPB surfactants at 2:1 wt:wt ratio; C12Ac, lauric acid; C14Ac, myristic acid; C16Ac, palmitic acid; CAPB, cocoamidopropyl betaine; cmc, critical micelle concentration; FAC, fatty acids; HSM, high surface modulus; IRRAS, Infra-Red Reflection Absorption Spectroscopy; LSM, low surface modulus; ODM, oscillating drop method; SLES, sodium lauryl-oxyethylene sulfate.

* Corresponding author. Tel.: +359 2 962 5310; fax: +359 2 962 5643.

E-mail addresses: sc@dce.uni-sofia.bg, SC@LCPE.UNI-SOFIA.BG (S. Tcholakova).

friction. The transitional pH value varies between 8 and 11, and increases with the fatty acid chain-length. The increase of pH causes ionization of the FAc molecules – the latter start to behave as usual anionic surfactant without forming surface condensed phase. The main effect of glycerol is to decrease the transitional pH (by 1 to 1.5 units for 40 wt% glycerol), without affecting significantly the system properties away from the transitional pH. These results clarify the compositional domain, in which the fatty acids can be used for control of surface and foam properties in such surfactant mixtures.

© 2012 Elsevier B.V. All rights reserved.

1. Introduction

The properties of monolayers of long-chain fatty acids (FAc) are widely studied in literature, due to the numerous applications of these acids (e.g., in detergency and personal care) and to the rich variety of surface phenomena being observed [1–20]. These studies showed that, upon compression, a phase transition in these monolayers may occur, and the transition point depends significantly on the chain length of the fatty acid, and on pH and temperature of the aqueous subphase.

X-ray diffraction and reflection studies provided information about the structure and composition of the adsorption layers. The experiments performed by Gericke and Hühnerfuss [4] with octadecanoic, hexadecanoic and pentadecanoic acids by infra-red reflection absorption spectroscopy (IRRAS) showed that the order of the hydrocarbon chains in the adsorption layer decreases with decreasing the chain-length, and this effect is more pronounced at pH = 6, compared to pH = 2. It was also shown that, upon compression or decrease of pH, the band in the IRRAS spectrum representing the double protonated carbonyl group is enhanced, which implied that the fatty acid molecules are linked by hydrogen bridges [4].

Similar conclusions about the structure of the adsorption layers were drawn by Wen et al. [11] who studied aqueous solutions of sodium myristate. In addition, these authors found that the surface tension of the sodium myristate solutions had a deep minimum at pH ≈ 8–9, being much higher at pH = 3 and pH = 12 [11]. IRRAS measurements showed [11] that the adsorption layer contains mainly unprotonated fatty acids at pH = 3, whereas the myristic anion is the main entity in the adsorption layer at pH = 12. It remains unclear why the measured surface tension is high at low pH values, at which protonated fatty acid molecules are expected to build up a dense adsorption layer [11].

In an independent study, Kralchevsky et al. [19] developed a theoretical model to determine the composition of the aggregates (micelles and precipitates), formed in the solutions of fatty acids and their sodium salts, from the measured dependence of pH on surfactant concentration. The surface tension isotherms of sodium dodecanoate (laurate) and sodium tetradecanoate (myristate) were measured and low surface tensions (≈23 mN/m) were measured only under conditions, where 1:1 acid soap precipitates were formed in the bulk solutions. The latter result suggests that mixed acid soap adsorption layers might be needed to observe such low surface tensions [19].

In recent studies [21–22] it was shown that maximum surface viscosity, foamability, and foam stability are observed around an optimal pH, near the pK_a of the respective fatty acid which, in turn, depends on the fatty acid chain length. For myristic acid pK_a is ≈9.5 and, as a consequence, there is almost no foam at lower pH [22]. It was shown also that at pH ≈ pK_a , the alkylcarboxylate solutions have very high surface elasticity [23], which has significant impact on dynamic foam properties, such as inside-foam friction [23], foam-wall friction [23–24] and bubble breakup in sheared foams [25].

In a previous study [26] we found that the addition at low pH ≈ 6.0 of fatty acids, as cosurfactants to the mixture of SLES and CAPB (low-molecular weight surfactants, described in Section 2), leads to a significant increase of the dilatational surface modulus

of the mixed surfactant solution [26]. This high surface modulus (HSM) was shown to affect significantly the dynamic properties of the foams formed from such triple surfactant mixtures, including foam rheological properties [26–27], the rate and mode of foam film thinning [26–27], and the rate of bubble Ostwald ripening [28]. It was demonstrated by several research groups [25–34] that these triple mixtures of SLES + CAPB + FAc are particularly suitable for systematic studies of the relation between the surface and foaming properties of the solutions, because the researchers may vary in wide range the solution surface modulus (between 3 and 400 mN/m), without encountering the specific difficulties when using solutions of pure fatty acids – bulk precipitation, slow changes of solution properties due to CO₂ absorption, reduced foaming at low and high pH, etc.

The current study is a direct continuation of our previous work [26], with a major aim to clarify the effects of (1) chain length of fatty acid, (2) fatty acid concentration, (3) pH, and (4) presence of glycerol in the triple mixture, on the surface properties (surface tension and surface modulus), foam rheological properties (inside-foam and foam-wall friction) and the related bubble size in sheared foams, formed from these solutions. Thus, we clarify the optimal conditions for using the long-chain fatty acids (as cosurfactants) to modify the surface properties of SLES + CAPB mixtures.

The article is organized as follows: Section 2 describes the materials and methods used. Experimental results are described in Section 3. Section 4 presents the discussion of the obtained results. The main results and conclusions are summarized in Section 5. List of used abbreviations is presented as footnote on the front page.

2. Materials and methods

2.1. Materials

The basic surfactant system, denoted as “BS”, is a mixture of the anionic surfactant sodium lauryl-oxyethylene sulfate, SLES (product of STEPAN Co., commercial name STEOL CS-170, molecular mass 332.4 g/mol) and the zwitterionic surfactant cocoamidopropyl betaine, CAPB (product of Goldschmith, commercial name Tego Betaine F50, molecular mass 356 g/mol), see Fig. 1S in the Supporting information for their molecular structures.

The following fatty acids were used: dodecanoic acid, C12Ac (product of Sigma–Aldrich, purity ≥ 98%); tetradecanoic acid, C14Ac (product of Sigma–Aldrich, purity ≥ 95%) and hexadecanoic acid, C16Ac (product of Riedel-de-Haën, purity ≥ 98%). All surfactants and fatty acids were used as received.

The procedure for preparation of the BS + fatty acid mixtures is as follows: first, we prepared concentrated stock solution of BS. The weight ratio of the active SLES and CAPB in the studied BS mixtures was fixed at 2:1 and the total surfactant concentration was $C_{TOT} = 10$ wt % (note that this weight ratio corresponds approx. to 2:1 molar ratio as well, because the molar masses of the two surfactants are similar). This composition was chosen because it represents the typical contents of many home and personal care formulations, such as shampoos, body washes and liquid detergents. In this concentrated solution we dissolved the fatty acid

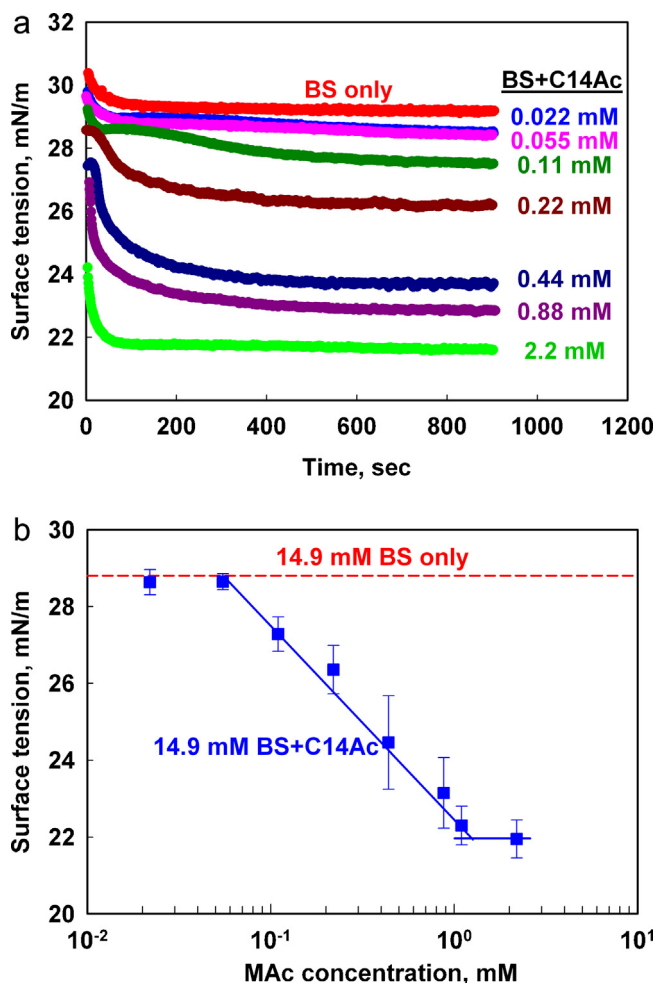


Fig. 1. (A) Kinetics of surface tension decrease for 15 mM BS (red symbols) and 15 mM BS + different concentrations of C14Ac, as indicated in the figure. (B) Equilibrium surface tension, σ ($t=900$ s), as a function of C14Ac concentration in the mixture. Experiments are performed at 20 °C. The error bars in (B) are calculated from, at least, three independent measurements and represent the standard deviation of the obtained results. (For interpretation of the references to colour in this figure legend, the reader is referred to the web version of this article.)

under mild stirring and heating, until a clear solution was formed. The solution was heated at 60 °C for dissolving myristic (C14Ac) and palmitic (C16Ac) acids, whereas heating at 45 °C was used for dissolving lauric acid (C12Ac).

For characterization of the surface and foam properties of the systems studied, the stock solutions were diluted 20 times with de-ionized water or with 40 wt% glycerol solution to prepare the final working solutions, used in the actual experiments. De-ionized water was obtained from Milli Q Organex water purification system. The pH of the working solutions was adjusted by adding small aliquots of 0.1 M NaOH or 0.1 M HCl solutions, prepared from NaOH with purity $\geq 95\%$ (product of Sigma–Aldrich) and HCl (32%, product of Sigma–Aldrich).

2.2. Measurements of viscosity and surface tension of the surfactant solutions

The viscosity of the diluted surfactant solutions, μ , was measured with thermostated capillary viscometer, after calibration with pure water. The surface tension of the foaming solutions, σ , was measured by Wilhelmy plate method on Tensiometer K100 (Kruss GmbH, Germany) at $T=20$ °C. Calibration with pure water was used before each series of experiments (at least once a day) for K100 instrument.

2.3. Measurements of surface dilatational modulus

The surface dilatational modulus of the surfactant solutions was measured by oscillating drop method (ODM) on DSA10 instrument, equipped with ODM/EDM module (Krüss, Germany). The principle of the method is the following: By using a piezo-driven membrane, small oscillations are generated in the volume of a pendant drop (hanged on a needle tip). These oscillations lead to periodical expansions/contractions of the drop surface area: $a(t) = a_0 \sin(\omega t)$, where $a(t) = [A(t) - A_0]/A_0$ is the normalized oscillation of the surface area around its mean value, A_0 , while a_0 is the relative amplitude and $\nu = \omega/2\pi$ is the frequency of oscillations. Video-images of the oscillating drop are recorded and analyzed by Laplace equation of capillarity to determine the resulting variation of the surface tension, $\sigma(t)$. For small deformations:

$$\sigma(t) = G_{SD} a_0 \sin(\omega t) + G_{LD} a_0 \cos(\omega t) \quad (1)$$

where G_{SD} is the surface storage modulus (related to surface dilatational elasticity) and G_{LD} is the surface loss modulus (related to surface dilatational viscosity, $\mu_{SD} = G_{LD}/\omega$). The total surface dilatational modulus is

$$G_D = (G_{SD}^2 + G_{LD}^2)^{1/2} \quad (2)$$

In our experiments, the oscillation frequency was fixed at $\nu=0.2$ Hz, the relative area amplitude was varied between 0.2 and 4%, and the temperature was maintained at $T=20$ °C using a thermostating chamber (model TC40, Krüss, Germany). At least 10 oscillation periods were used in each measurement.

2.4. Foam generation for rheological measurements

To generate foam with air volume fraction, $\Phi \approx 90\%$, we used the following procedure: First, 1 mL surfactant solution was sucked into a 20 mL syringe, equipped with a stainless steel needle with 2.5 mm internal diameter (Hamilton, Cat. no. 7730-05). Then, 9 mL air was captured in the syringe, forming coarse foam with large bubbles. These large bubbles were broken into much smaller bubbles, by using a series of multiple ejection/injection cycles of the foam through the needle.

In this way, foams with $\Phi \approx 90 \pm 1\%$ (measured gravimetrically, Section 2.6) and containing bubbles of sub-millimeter diameter, were produced. Next, these foams were sheared in a rheometer (see Section 2.7 below) for 2 min, at shear rate of 200 s^{-1} , to break the initial bubbles into smaller ones, under controlled shear rate [25]. The bubble size distribution and the mean bubble size, R_{32} , were measured immediately after stopping the foam shear, as described in Section 2.5.

The reproducibility in the mean bubble size of the formed foams was found to be ± 10 to 15% – see, e.g., the error bars in Fig. 6a below which represent the standard deviation, determined from measurements of three independent foam samples for given conditions.

2.5. Determination of bubble size distribution and average bubble size

Bubble size distribution was determined by using the procedure of Garrett et al. [35–36], Fig. S2 in Supplementary materials. The foam was spread in a small petri dish and an optical triangular prism was placed on top of the plate, in direct contact with the foam. The foam was illuminated by diffuse white light through one of the prism side-walls, whereas the foam observation was made by video-camera, through the other side-wall of the prism. In the recorded images one sees as bright polygonal spots the wetting films, formed between the bubbles and the prism wall, whereas the Plateau borders around the films are seen as dark interconnected

areas. The foam images were processed via a shareware computer program Image J, released by the National Institute of Health (NIH).

In the first stage of image processing, the original image is converted into black-and-white image with appropriate threshold of the gray levels, see image B in Fig. S2. Next, the plateau borders are diminished down to 3 pixels width (image C in Fig. S2) and in this way, a projection of the outer contour of the bubbles on the prism wall is obtained. Image J program allows one to determine the projected area of each bubble, A_B . As the foam is observed under a certain angle with respect to prism wall, $\alpha \approx 45^\circ$, the bubbles in the image appear shortened along one of the axes by a factor $\cos\alpha$. Therefore, the values of A_B are first corrected by dividing the observed bubble projected area with $\cos\alpha$, and next the bubble radii are calculated as $R_B \approx (A_B/\pi)^{1/2}$, for each bubble seen in the image. In this way, one can construct the bubble-size distribution histograms and determine the mean volume-surface radius, $R_{32} = \sum_i R_{Bi}^3 / \sum_i R_{Bi}^2$. At least 1500 bubbles for a given sample were analyzed to determine R_{32} .

2.6. Determination of air volume fraction in foam, Φ

The air volume fraction was determined gravimetrically: syringe with a known volume (20 mL) was filled with foam and weighted. The air volume fraction, Φ , is determined from the relation $\Phi = 1 - m_F/(V_F\rho)$, where m_F is the mass of the foam in the syringe, V_F is the volume of this foam, and ρ is the mass density of the foaming solution.

2.7. Characterization of foam rheological properties

Rheological properties of the studied foams were determined with Gemini rotational rheometer (Malvern Instruments, UK), in parallel plate geometry, at temperature of 20 °C.

Two types of experiments were performed – friction inside sheared foam and foam-wall friction. In the first type of experiments, sandpaper (P100) was glued on both plates of the rheometer to suppress foam-wall slip. During the experiment, the shear rate, $\dot{\gamma}$, was varied logarithmically from 0.02 s⁻¹ to 200 s⁻¹ and the shear stress was recorded, $\tau = \tau(\dot{\gamma})$. In this case, the stress measured by the rheometer was due to viscous dissipation in the bulk of the foam (bubble/bubble friction). All these experiments were performed after an initial pre-shear of the foam samples for 2 min at 200 s⁻¹.

In foam-wall friction experiments, sandpaper (P100) was glued only on the lower plate, whereas a smooth glass plate was glued on the upper (rotating) plate. In this way, there was no slip between the foam and the lower plate, whereas the foam slipped over the upper plate. During these experiments, the shear stress is kept below the foam yield stress to prevent shear flow in the bulk foam. In this way, we can measure the shear stress which is due entirely to the viscous friction of the foam with the confining smooth solid wall (foam-wall friction).

All experiments were performed by using parallel plates with radius of 20 mm, and gap-width of 3 mm. Control experiments at smaller gaps (down to 1.5 mm) did not show any noticeable dependence of the measured rheological properties on the gap-width. No larger gaps were used to avoid possible effects of water drainage from the foam, which could compromise the rheological results.

The obtained results for the dependence of the total shear stress on the rate of strain for steadily sheared foams were described very well by Herschel–Bulkley model, which includes three parameters – yield stress, t_0 ; consistency, k ; and power-law index, n :

$$\tau = \tau_0 + \tau_V(\dot{\gamma}) = \tau_0 + k\dot{\gamma}^n \quad (3)$$

Here $\dot{\gamma}$ is the applied shear rate, τ is the total shear stress, and τ_V is the rate-dependent component of the stress (called for brevity “viscous stress”). As discussed in literature [37–43], it is appropriate to scale the yield stress and viscous stress by the bubble capillary pressure, $P_C \sim \sigma/R_{32}$, whereas the shear rate is adequately represented by the dimensionless capillary number, Ca :

$$\tilde{\tau}_0 = \frac{\tau_0}{(\sigma/R_{32})}; \tilde{\tau}_V = \frac{\tau_V}{(\sigma/R_{32})}; Ca = \frac{\mu\dot{\gamma}R_{32}}{\sigma} \quad (4)$$

Here $\tilde{\tau}_0$ is dimensionless yield stress, $\tilde{\tau}_V$ is dimensionless viscous stress, and R_{32} is mean volume-surface radius, while σ is surface tension and μ is viscosity of the foaming solution.

The fits to the experimental data by Herschel–Bulkley model, Eq. (3), allowed us to determine the three parameters of this model with the following reproducibility: $\pm 15\%$ for τ_0 , $\pm 10\%$ for k , and ± 0.02 units for n .

For scaling of the results for foam/wall friction, the dimensionless velocity of the foam with respect to the moving plate and the respective dimensionless foam-wall stress are used [23]:

$$\tilde{V}_W = \frac{\mu V_W}{\sigma} \quad (5)$$

$$\tilde{\tau}_W = \frac{\tau_W}{\sigma/R_{32}} \quad (6)$$

3. Experimental results

In this section we present experimental results about the effects of the studied factors on the surface properties (Section 3.1), mean bubble size after foam shearing at high shear rate (Section 3.2), and foam rheological properties (Section 3.3). All these results are discussed within a common mechanistic framework in the following Section 4.

3.1. Surface properties

The solution surface properties are characterized with respect to dynamic surface tension, equilibrium surface tension, and surface dilatational modulus. The obtained results are presented in the following order: The effect of C14Ac concentration at pH = 6 is presented in Section 3.1.1. The results about the effect of pH variation are described in Section 3.1.2. The effects of fatty acid chain-length and addition of glycerol are presented in Section 3.1.3.

3.1.1. Effect of C14Ac concentration at pH = 6

The effect of C14Ac concentration on the solution surface properties was studied at fixed concentration of the main surfactants SLES + CAPB, $C_{BS} = 15$ mM, which is ≈ 30 times above the critical micelle concentration (cmc) of this solution. The cmc was determined by measuring the surface tension isotherm of mixed SLES + CAPB solutions, at fixed ratio of the two surfactants (2:1 by weight). For comparison, the cmc values of the individual surfactants are 0.7 mM for SLES and 0.09 mM for CAPB.

The C14Ac concentration in the solutions was varied between 0.022 and 2.2 mM, which means that it was at least 6 times lower than that of the main surfactants. Therefore, C14Ac can be considered as a cosurfactant in these solutions.

The results for the dynamic surface tension, measured at different C14Ac concentrations, are compared in Fig. 1A. One sees that the presence of C14Ac in the solutions does not affect significantly the dynamic surface tension of BS solution at low C14Ac concentrations, $C_{C14Ac} \leq 0.055$ mM. At $C_{C14Ac} = 0.11$ mM, the dynamic surface tension starts almost from the same value as that of the BS solution, remains ≈ 28.7 mN/m during the first 150 s, and decreases noticeably afterwards. Qualitatively similar behavior is observed

at $C_{\text{C14Ac}} = 0.22$ mM, with shorter lag-time of ≈ 30 s. The further increase of C14Ac concentration to 0.44 mM leads to lower starting σ and even shorter lag-time. No lag-time is observed at higher C14Ac concentrations, $C_{\text{C14Ac}} \geq 0.88$ mM. See Section 4 below for explanations of these trends.

The surface tension of BS + C14Ac solutions measured 900 s after surface formation (close to the equilibrium surface tension of the solutions) is shown in Fig. 1B. One sees that σ for BS + C14Ac, at $C_{\text{C14Ac}} \leq 0.055$ mM, is very close to the equilibrium surface tension of BS solution, ≈ 28.7 mN/m. Further increase of C_{C14Ac} leads to significant lowering of the equilibrium surface tension down to 22 mN/m at $C_{\text{C14Ac}} = 1$ mM, remaining around the latter value at higher C14Ac concentrations. As shown in Fig. 1B, the surface tension of BS + C14Ac solutions decreases linearly with the logarithm of C14Ac concentration in the range between 0.08 mM and 1 mM. The slope of this dependence is $d\sigma/d\ln C_{\text{C14Ac}} \approx -2$ mN/m. This slope cannot be related directly to the adsorption of C14Ac molecules, due to the presence of the main surfactants, SLES and CAPB, in the adsorption layer (see Section 4 for further discussion of this result).

The results for the surface dilatational modulus of the mixed solutions, as a function of C14Ac concentration, are shown in Fig. 2.

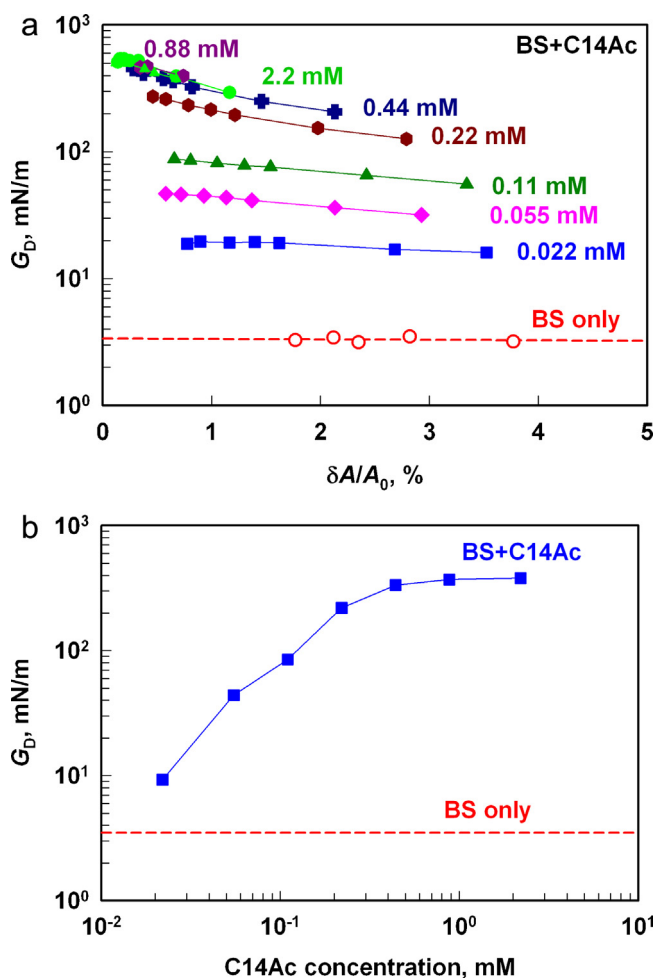


Fig. 2. (A) Surface modulus, as a function of surface deformation for BS (red symbols) and BS + C14Ac solutions, at different C14Ac concentrations as indicated in the figure. (B) Surface modulus, as a function of C14Ac concentration in the mixture, at $\delta A/A_0 = 0.8\%$. In all experiments the concentration of BS is 15 mM, $T = 20^\circ\text{C}$, period of oscillation = 5 s, and the surface layer is aged for 900 s before starting the oscillations. Each experimental curve (for given solution composition) is compiled from the results obtained in three independent experiments; therefore, the scattering of the experimental points reflects the measurement reproducibility. (For interpretation of the references to colour in this figure legend, the reader is referred to the web version of this article.)

First, we should notice that the surface modulus of BS + C14Ac solutions may depend significantly on the oscillation amplitude (at given frequency of oscillations), while the modulus of BS solution is virtually independent of this amplitude – see Fig. 2A. This non-linear response of the adsorption layer is more pronounced at high C_{C14Ac} and is probably due to: (i) exchange of adsorbing molecules with the underlying bulk solution, viz. variations in the layer composition, which might depend on the amplitude of surface deformation, and/or (ii) changes in the structure of the adsorption layer upon large relative deformations. At the current moment we have no sufficient information to favor or discard any of these explanations.

The effect of C14Ac concentration on the surface modulus, see Fig. 2B, is discussed for 0.8% amplitude of surface oscillations, which falls in the range of estimated surface area deformations for the bubbles in sheared foams [37]. One sees from Fig. 2B that the surface modulus increases from 10 mN/m up to 380 mN/m, with the increase of C14Ac concentration from 0.022 mM to 0.44 mM, and remains almost constant at higher C14Ac concentrations. It should be mentioned that even at the lowest studied concentration, $C_{\text{C14Ac}} = 0.022$ mM, the surface modulus of BS + C14Ac solutions (10 mN/m) is significantly higher than that of BS solution (3.5 mN/m). The latter comparison evidences that even at very low C14Ac concentrations, when the surface tension is apparently unaffected by C14Ac (cf. Fig. 1B), the surface modulus is increased significantly by the C14Ac molecules. The initial reduction of the surface tension by C14Ac at $C_{\text{C14Ac}} \approx 0.1$ mM is associated with rather high surface modulus, $G_D > 50$ mN/m.

From this series of experiments we can conclude that the increase of C14Ac concentration in BS mixture at pH = 6 leads to a significant decrease of surface tension (down to 22 mN/m) and significant increase of surface modulus (up to 380 mN/m at $\delta A/A_0$ 1% and 5 s period of oscillation). The time required for formation of surface condensed phase in the adsorption layer, with the related low surface tension and high modulus, decreases from 150 s down to 30 s while increasing C_{C14Ac} from 0.11 to 0.22 mM.

3.1.2. Effect of pH for BS+C14Ac solutions

The effect of pH was studied with 15 mM BS + 0.88 mM C14Ac and 15 mM BS + 2.2 mM C14Ac solutions. After adjusting the pH, these solutions were homogenized by stirring for 5 min at 150 rpm before measuring their surface properties. The pH of these solutions was measured again after their surface characterization and the deviations from the initial pH were less than 0.1 pH units.

The experimental results for $\sigma(t)$, obtained with 15 mM BS + 0.88 mM C14Ac solutions, are shown in Fig. 3A. One sees that the dynamic surface tension depends significantly on pH. At pH = 3, σ starts from 25.7 mN/m, remains almost constant for 25 s, decreases down to 23.3 mN/m in the following 200 s, and remains almost constant afterwards. The surface tension at pH = 6 starts from higher value, 27 mN/m, and decreases gradually down to 23 mN/m for 900 s. The increase of pH from 6 to 8 leads to further increase of the initial and final values of σ (28.3 and 24.2 mN/m, respectively). No lag-time is observed at pH = 6 and 8 in the curve $\sigma(t)$. The increase of pH from 8 to 9 leads to a significant increase of the initial σ up to 31 mN/m, well pronounced plateau (lag-time) of around 200 s, where the surface tension remains ≈ 28.7 mN/m, and slow further decrease of σ down to 26 mN/m after 2000 s. The lag-time is even more pronounced at pH = 10 and pH = 11 (900 and 1500 s, respectively) – see Fig. 3A. Concluding, the increase of pH leads to significant increase of the initial and final surface tensions of the solutions, and to longer lag-times.

The surface tensions reached after 900 s, at the two C14Ac concentrations studied, are compared in Fig. 3B for different pH values. One sees that, at $C_{\text{C14Ac}} = 2.2$ mM, the surface tension remains almost constant in the pH range between 3 and 8, starts to increase

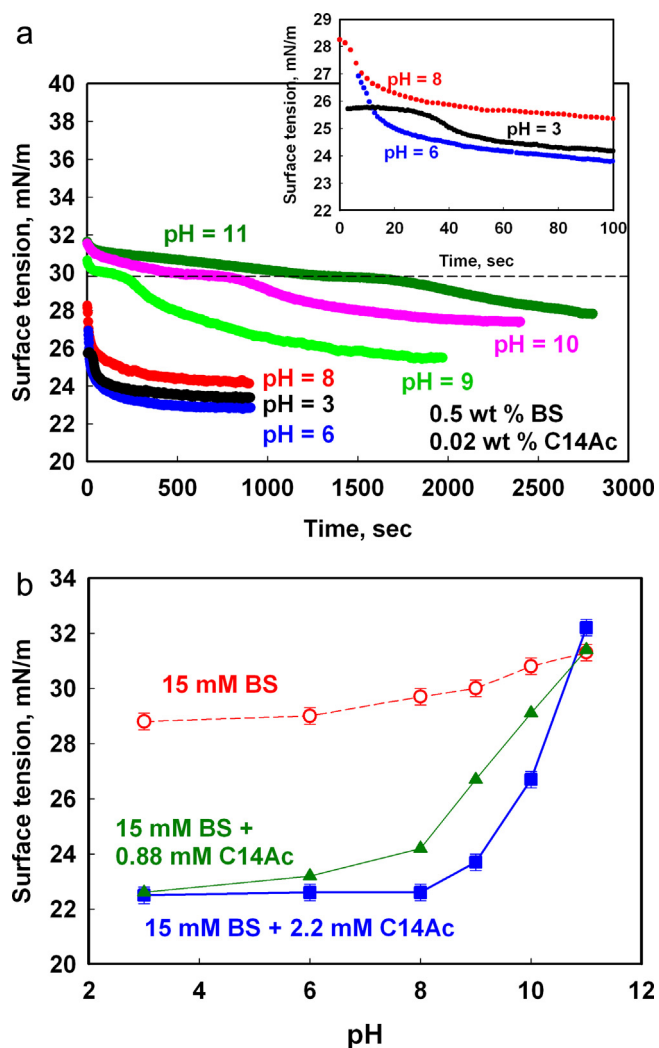


Fig. 3. (A) Kinetics of surface tension decrease for 15 mM BS + 0.88 mM C14Ac at different pHs as indicated in the figure. The inset blows the short-time data for pH = 3, 6 and 8. (B) Surface tension as a function of pH for 15 mM BS (red symbols); 15 mM BS + 0.88 mM C14Ac (green triangles) and 15 mM BS + 2.2 mM C14Ac (blue squares). Surface tension is measured after 900 s at $T = 20 \pm 1^\circ\text{C}$. The pH of the solutions after measurements did not differ by more than 0.1 pH units, compared to the initial one. The error bars in (B) are calculated from, at least, three independent measurements and represent the standard deviation of the obtained results. (For interpretation of the references to colour in this figure legend, the reader is referred to the web version of this article.)

at pH=9 and reaches the value for BS (without C14Ac) at pH=11. Similar behavior is observed at the lower C14Ac concentration, $C_{\text{C14Ac}} = 0.88\text{ mM}$. However, in the latter case σ starts to increase at pH=8. This dependence of σ on pH is certainly related to the degree of protonation of the C14Ac molecules in the solution, viz. to the pK_a value of the fatty acid. Further discussion of this dependence is given in Section 4.

The surface moduli of BS + C14Ac solutions, at $C_{\text{C14Ac}} = 0.88\text{ mM}$ and different pH values, are compared in Fig. 4A. In this series of experiments, the surface oscillations were applied after 900 s of surface formation. One sees that the measured surface modulus at pH=6, 8 and 9 are the same in the frame of our experimental accuracy (380 mN/m), while the surface modulus at pH=3 is somewhat lower (270 mN/m). The surface modulus at higher pH (10 and 11) decreases significantly and approaches that of the BS solution (without FAC). Note that the surface tension increases from 22.8 to 26.7 mN/m while increasing pH from 3 to 9, while the surface modulus does not change significantly in this pH range. Interestingly,

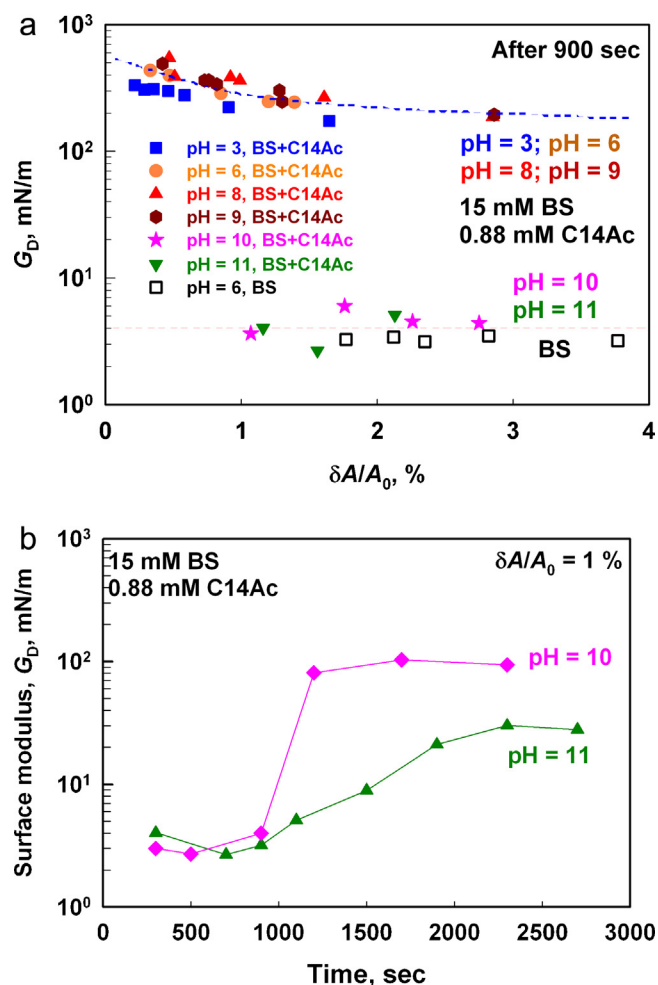


Fig. 4. (A) Surface modulus, G_D , as a function of relative surface deformation, measured after 900 s of drop formation for 15 mM BS + 0.88 mM C14Ac, at different pHs, as indicated in the figure. The empty squares represent data for the reference system, BS (no additive). (B) Surface modulus, G_D , as a function of surface age for 15 mM BS + 0.88 mM C14Ac at pH=10 (pink diamonds) and pH=11 (green triangles). The surface modulus of the reference BS solution was constant in the time-frame of these experiments, $G_D = 4 \pm 1\text{ mN/m}$. All experiments are performed at period of oscillations = 5 s and $T = 20^\circ\text{C}$. The experimental curves in (A) are compiled from the results obtained in three independent experiments – the scattering of the experimental points reflects the measurement reproducibility. Each curve in (B) is obtained from a single experiment. (For interpretation of the references to colour in this figure legend, the reader is referred to the web version of this article.)

the further increase of surface tension from 26.7 to 29.1 mN/m at higher pH (10 to 11) leads to more than 100-fold decrease of surface modulus. Therefore, somewhat unexpectedly, no direct correlation between the variations of the surface tension and the surface modulus of these solutions is observed.

We can conclude from these results that the observed step-wise transition in the surface modulus upon increase of pH from 9 to 10 is related to a significant change in the adsorption layer structure (surface phase transition) which is not reflected in a similar step-wise change in the solution surface tension (cf. Fig. 1B and Fig. 4A).

As far as the measured surface moduli after 900 s for pH=10 and 11 are before the end of the plateau regions in the respective $\sigma(t)$ curves (see Fig. 3A), we made additional measurements at different aging times of the surface. The obtained results are shown in Fig. 4B. One sees that, for pH=10, G_D increases sharply from 4 mN/m up to 100 mN/m between 900 and 1200 s, which is in a good agreement with the observed kink in the $\sigma(t)$ curve, cf. Fig. 3A. Interestingly, we did not observe a further increase of the surface modulus after 1200 s of aging time, while the surface ten-

sion continued to decrease at long aging times. At pH = 11, a gradual increase of the surface modulus is observed with time. After 2500 s, the surface modulus approaches ≈ 30 mN/m and no further increase is observed afterwards.

From this series of experiments we can conclude that the increase of pH above 6 leads to a gradual increase of surface tension, step-wise decrease of surface modulus (between pH=9 and 10) and gradual increase of the time required for formation of surface condensed phase in the adsorption layer. At pH = 10, surface condensed phase is formed after 1200 s with surface modulus of ≈ 100 mN/m. At pH = 3, the surface condensed phase is with surface modulus of ≈ 270 mN/m, which is somewhat lower than the surface modulus measured in the pH range 6 to 9 (≈ 380 mN/m). At pH = 11, the adsorption layer has much lower surface modulus, it is ≈ 30 mN/m even after 2500 s.

3.1.3. Effect of fatty acid chain length and glycerol

In this section we present results about the effect of fatty acid chain-length and glycerol on the surface tension and surface modulus of BS solutions, at different pH values and two fatty acid concentrations. The effects of lauric acid (C12Ac); 1:1 mixture of lauric and myristic acids (C12Ac + C14Ac), and palmitic acid (C16Ac) were studied with respect to the dependence $\sigma(\text{pH})$ and to the surface modulus, at pH=6. The concentration of BS was fixed to 15 mM. The studied concentrations of fatty acids were 0.05 wt% and 0.025 wt%. The higher weight concentration corresponds to 2.5 mM of C12Ac and 1.95 mM of C16Ac. Note that both types of comparison of the fatty acids make sense and are explored in Section 3, at fixed weight concentration and at fixed molar concentration.

The results for the surface tension of the solutions after 900 s are shown in Fig. 5A and in Fig. S6 in the Supplementary material. One sees that the surface tension of the reference system, BS (without FAc), increases from 29.0 mN/m to 31.4 mN/m with the increase of pH from 6 to 11. To understand the reason for the increased surface tension of the BS solution, we measured σ for 10 mM SLES and 5 mM CAPB at pH=6 and pH=10. The surface tension of SLES solution was 33.8 mN/m at both pH values tested. On the other hand, σ for CAPB increased from 27.8 mN/m at pH=6 up to 35.5 mN/m at pH=10. Therefore, the observed increase of σ for the BS mixture is probably due to changes in the CAPB adsorption. There is no significant effect of glycerol on the dependence σ vs pH for the BS solution, cf. the full and empty red circles in Fig. 5A.

The surface tension for BS + C12Ac solution, without glycerol, increases gradually from 23.5 to 31.3 mN/m, while increasing pH from 6 to 11. In presence of glycerol, σ of the same surfactant mixture increases steeply from 23.3 to 28.5 mN/m while increasing pH from 6 to 8, followed by a much slower increase at higher pH, see the green triangles in Fig. 5A. When C12Ac + C14Ac mixture, C14Ac and C16Ac are used as cosurfactants, σ remains almost constant ≈ 22.5 mN/m up to a given pH, and increases step-wisely afterwards. For C14Ac and the mixture C12Ac + C14Ac the critical value of pH is ≈ 9 , whereas it is ≈ 11 for C16Ac (Fig. S6). The addition of glycerol in these solutions increases noticeably σ in the intermediate pH range and does not affect significantly σ at low and high pH values, cf. the empty and full symbols in Fig. 5A. Most probably, the glycerol in these solutions affects the hydrogen bond formation between the components of the mixed adsorption layer, thus influencing the surface tension, surface modulus and the transitional pH.

To clarify the effect of FAc chain length on the surface modulus, we measured the surface modulus of different mixtures at pH=6, see Fig. 5B. One sees that the surface modulus increases from 160 mN/m up to 780 mN/m with the increase of the FAc chain length from C12 to C16. Therefore, the cohesive energy between the ordered surfactant-cosurfactant tails has a very significant con-

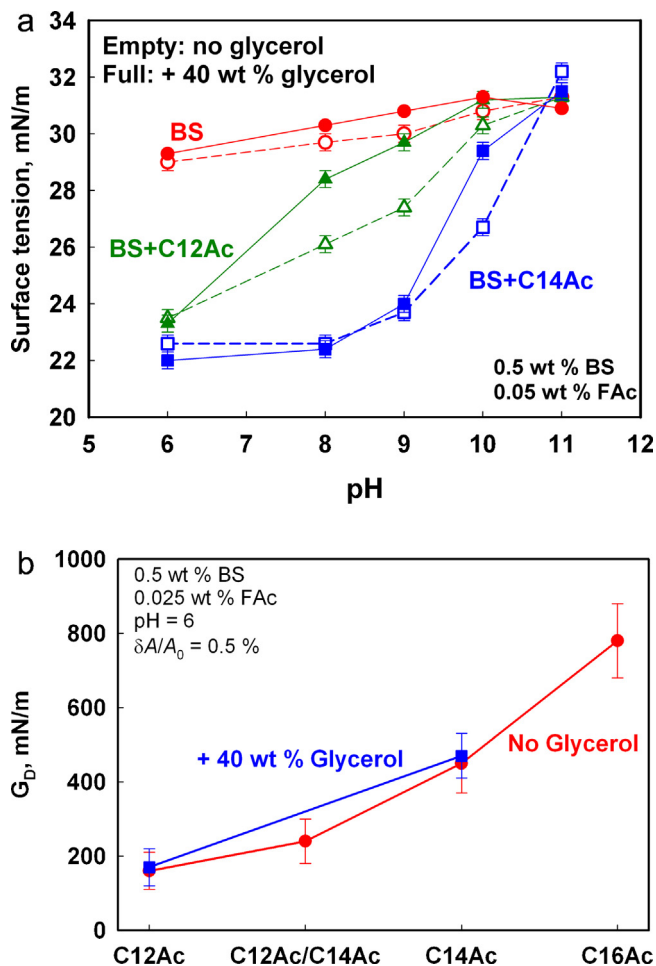


Fig. 5. (A) Surface tension as a function of pH for 15 mM BS + 0.05 wt% FAc (empty symbols) and 15 mM + 0.05 wt% FAc + 40 wt% glycerol (full symbols). Different symbols correspond to different fatty acids, as indicated in the figure. (B) Surface modulus as a function of chain length of fatty acid without (red circles) and with 40 wt% glycerol (blue symbols). Experiments are performed with 15 mM BS + 0.025 wt% FAc at pH = 6. The presented values are determined at period of oscillations = 5 s, surface deformation of 0.5%, and $T = 20$ °C. The error bars are calculated from, at least, three independent measurements and represent the standard deviation of the obtained results. (For interpretation of the references to colour in this figure legend, the reader is referred to the web version of this article.)

tribution to the magnitude of the measured surface modulus. No significant effect of glycerol is detected at pH = 6 (Fig. 5B).

From this series of experiments we can conclude that the surface tension of all studied solutions increases with the increase of pH. Gradual increase is observed for C12Ac-containing solutions, whereas sharper step-wise increase is observed for the fatty acids with longer tails. The transitional pH, above which the surface tension becomes higher than 26 mN/m, increases with the chain-length and the concentration of the fatty acids and decreases with the addition of glycerol.

3.2. Mean bubble size in formed foams

As shown in our previous studies, there is a relation between the surface rheological properties of the foaming solutions, the rheological properties of the respective foams, and the mean bubble size after shearing at high shear rates of these foams [23–28]. In the current study we track these relations for the BS + FAc mixed systems. Foams with 90% bubble volume fraction were sheared in the rheometer for 2 min, at 200 s $^{-1}$ shear rate, to break the initial large bubbles into smaller ones – for the mechanism of this process

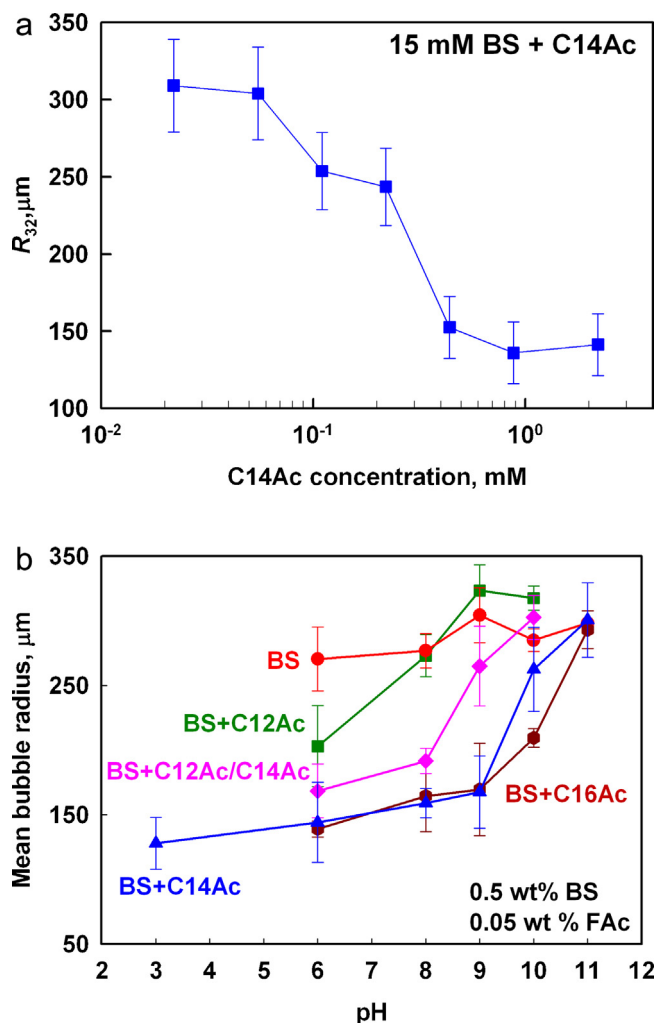


Fig. 6. Mean bubble size, as a function of (A) C14Ac concentration and (B) pH for BS + FAc mixtures. Different symbols correspond to different fatty acids added as cosurfactants, as indicated in the figure. In all experiments the concentration of BS is 15 mM = 0.5 wt% (10 mM SLES + 5 mM CAPB). The error bars represent the standard deviation of the measured mean bubble size in, at least, 3 independent experiments. In each experiment, 500 bubbles are measured.

see Ref. [25]. The bubble size distribution and the mean bubble size, R_{32} , were measured immediately after stopping the foam shear, as described in Section 2.5.

In Fig. 6A we present experimental results for the mean bubble size, R_{32} , as a function of C14Ac concentration in the triple mixture. One sees that R_{32} decreases from 300 μm to 150 μm with the increase of C14Ac concentration from 0.055 mM to 0.44 mM (and remains constant at higher C14Ac concentrations). At low C14Ac concentrations, $C_{\text{C14Ac}} \leq 0.022$ mM, R_{32} is the same as that for BS solutions. Noticeable decrease of R_{32} from 300 to 250 μm is observed for $C_{\text{C14Ac}} = 0.11$ mM, while R_{32} for solutions containing 0.22 mM C14Ac (240 μm) is similar to that for 0.11 mM C14Ac. Additional sharp decrease of bubble size is observed at 0.44 mM C14Ac, $R_{32} \approx 150$ μm . Thus we observe two steps in the dependence $R_{32}(C_{\text{C14Ac}})$ – at 0.11 mM and at 0.44 mM C14Ac. The interpretation of these results is presented in Section 4.

The obtained results for the effect of pH on R_{32} are shown in Fig. 6B, for the various fatty acids studied. One sees that R_{32} remains almost constant (≈ 290 μm) while varying the pH for BS solution. In contrast, a gradual increase in R_{32} from 160 μm to 290 μm is observed for BS + C12Ac solutions, while increasing pH from 6 to 10. The mean bubble size in foams formed from BS + C12Ac + C14Ac and

BS + C14Ac solutions is almost the same at pH = 6 and 8 (≈ 150 μm for C14Ac and ≈ 160 μm for C12Ac + C14Ac) and increases gradually upon further increase of pH up to the mean bubble size for BS solution. Similar behavior is observed for C16Ac-containing solutions: $R_{32} \approx 140$ μm for pH up to 9 and increases afterwards. Summarizing, R_{32} increases gradually in a certain pH range, from the typical value for bubbles with high surface modulus (≈ 150 μm) to the typical values for the BS solution with low surface modulus (≈ 290 μm).

As a rule, the addition of glycerol to the foaming solution leads to significantly smaller values of R_{32} , due to the higher viscous friction in the presence of glycerol, see Ref. [25] for explanation of this effect. The mean bubble size for BS + glycerol foams is $R_{32} \approx 150$ μm , whereas for the solutions containing both FAc and glycerol $R_{32} \approx 100$ μm . The effect of pH on R_{32} in the presence of glycerol is demonstrated in Fig. S3 – again, R_{32} increases with the increase of pH, reaching the typical value for BS stabilized foams.

Concluding, a strong relation exists between the surface properties and the mean bubble size in sheared foams. The foaming solutions with high surface modulus give much smaller bubbles, compared to the solutions with low surface modulus.

3.3. Foam rheological properties

In this section we present experimental results about (1) effect of C14Ac concentration on inside-foam friction and foam-wall friction at pH = 6 in Section 3.3.1, (2) role of pH for BS + C14Ac stabilized foams in Section 3.3.2, and (3) effects of the fatty acid chain length and glycerol in Section 3.3.3.

3.3.1. Effect of C14Ac concentration on foam rheological properties at pH = 6

In Fig. 7 we present results for the dimensionless viscous friction in foams and the dimensionless foam-wall stress, as functions of the capillary number and dimensionless velocity, respectively, for foams stabilized by BS + C14Ac mixture. Data for the reference system BS (no additives) are also shown for comparison. In Fig. 7A we see that the results for the dimensionless foam stress group around two master lines with $n \approx 0.23$ and $n \approx 0.42$. At $C_{\text{C14Ac}} \leq 0.055$ mM, the viscous stress is the same as that measured with BS without additives, $n \approx 0.42$. At higher C14Ac concentrations, $C_{\text{C14Ac}} \geq 0.22$ mM, we measured $n = 0.23$ and much higher viscous friction. This result shows that a minimal concentration of $C_{\text{C14Ac}} \geq 0.22$ mM is needed to achieve a transition in the foam friction regimes. Unlike the experiments with the surface tension, where σ decreases gradually, in the experiment with foam viscous friction we observe a sharp transition within a relatively narrow range of C14Ac concentrations (between 0.11 and 0.22 mM). Note that the mean bubble size is almost the same for these two concentrations of C14Ac, $R_{32} \approx 240$ μm , whereas the measured surface moduli are rather different, 80 mN/m and 220 mN/m, respectively. The later observation is explained in Section 4.

Experimental results for the foam-wall friction are shown in Fig. 7B. One sees that the transition from tangentially mobile bubble surfaces, which are characterized with power law index of $m = 2/3$, to tangentially immobile bubble surfaces characterized with $m = 1/2$ [23,27], occurs again at C_{C14Ac} between 0.11 and 0.22 mM.

Therefore, the increase of the surface modulus above ca. 100 mN/m, with the increase of C_{C14Ac} , results in a sharp step-wise transition in the regime of viscous dissipation in sheared foams. Note that this surface modulus is measured at low oscillation frequency, $\nu = 0.2$ Hz, thus reflecting only the “rigidity” of the adsorption layers containing fatty acids. Our experimental method does not allow one to determine the dependence of the surface modulus on the oscillation frequency, at higher frequencies which would be more relevant to bubble deformations in sheared foams.

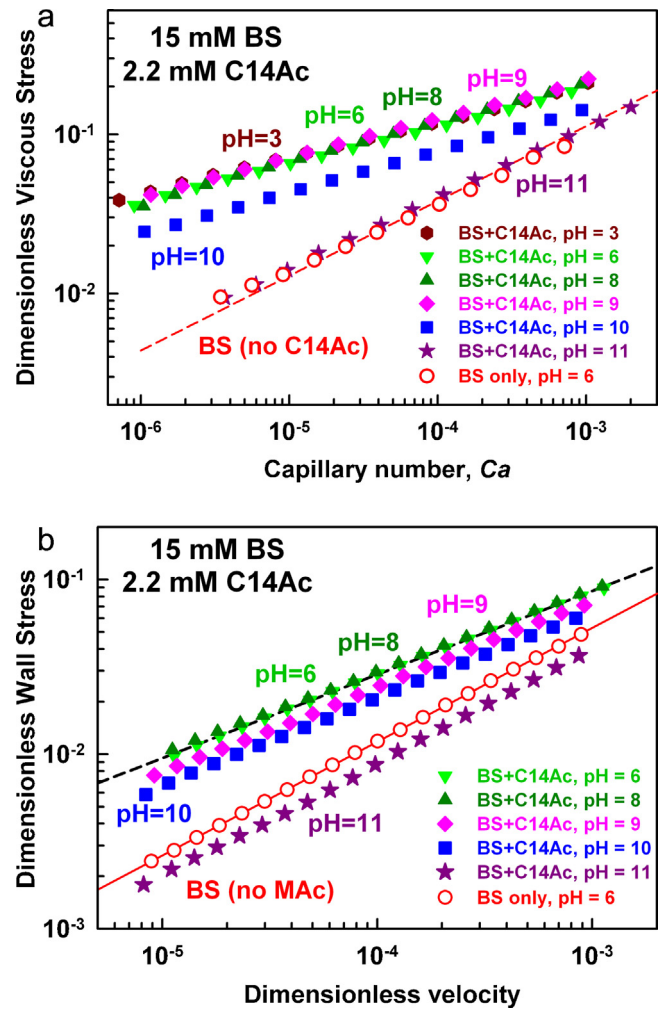
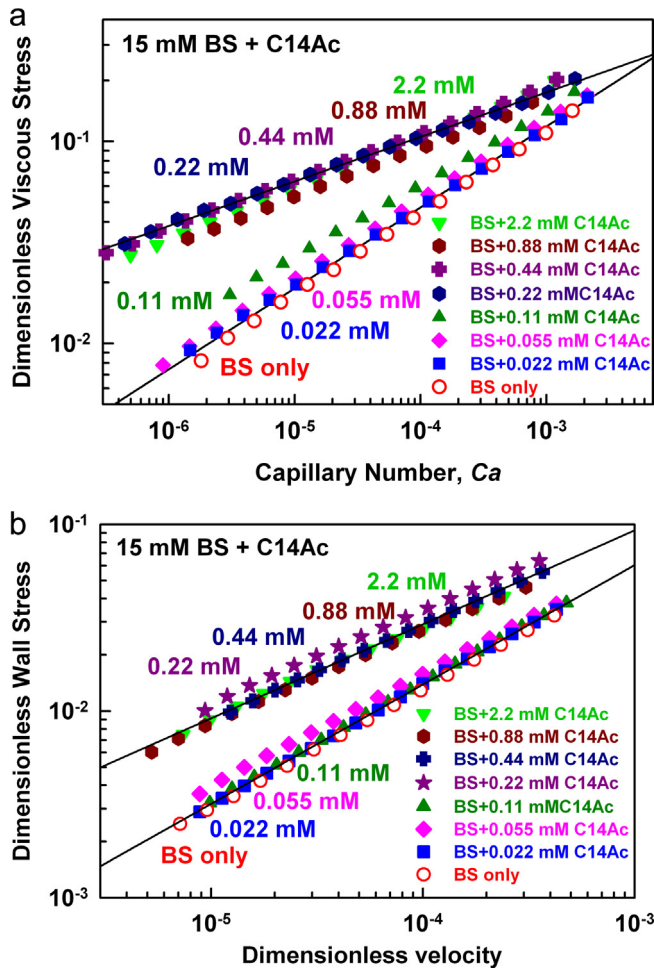


Fig. 7. (A) Dimensionless viscous stress as a function of capillary number, Ca and (B) Dimensionless wall stress as a function of dimensionless velocity, for foams formed from 15 mM BS and different concentrations of C14Ac, as indicated in the figure. The empty red symbols represent data obtained with foams formed from 15 mM BS (no additive). (For interpretation of the references to colour in this figure legend, the reader is referred to the web version of this article.)

Fig. 8. (A) Dimensionless viscous stress, as a function of capillary number, Ca and (B) Dimensionless wall stress, as a function of dimensionless velocity, for foams formed from 15 mM BS + 2.2 mM C14Ac at different pHs as indicated in the figure. The empty red symbols represent data obtained with foams formed from 15 mM BS (no additive). (For interpretation of the references to colour in this figure legend, the reader is referred to the web version of this article.)

Therefore, we use the measured surface modulus only as a simple “discriminator” for the two types of systems encountered in these studies (with high and with low surface moduli, respectively). The detailed mechanistic explanation of the observed regime of foam friction in the systems with high surface modulus would require more elaborated measurements at higher frequency and much deeper theoretical analysis.

3.3.2. Effect of pH for foams formed from 15 mM BS + 2.2 mM C14Ac

We first measured the viscous friction in foams formed from BS solution, as a reference. In Fig. S4 of the Supplementary material we present the dimensionless viscous stress, as a function of the capillary number, for foams stabilized with BS (with and without 40 wt% glycerol present), as measured at various pH values. All experimental results, obtained at different pH values and viscosities of the foaming solutions, are described by a single master line when presented in dimensionless form. The power-law index is $n \approx 0.42$, very close to the one expected for bubbles with low surface modulus. The experimental value of n is slightly lower than the theoretical value $n \approx 0.47$ [37]. The reason for this difference could be small amounts of fatty acids, present as contaminants in CAPB (remaining from the synthesis of this surfactant). Despite this difference, the measured value of n indicates that the

energy dissipation occurs predominantly in the foam films [37,49] (negligible surface dissipation) in these systems, regardless of the solution pH.

In Fig. 8 we present experimental results about the inside-foam and foam-wall viscous friction, for foams from BS + C14Ac solution. One sees that the dimensionless viscous stress does not depend on pH, when the latter is varied between 3 and 9. The viscous friction in foams formed at pH = 10 is somewhat lower than that at the lower pH values. The further increase of pH up to 11 leads to a significant reduction of the viscous friction, and the results merge with those obtained with BS solution without additives. Therefore, the transitional pH, at which the regime of viscous friction in foams changes, is between 10 and 11 for this C14Ac concentration (2.2 mM). Additional experiments were performed at lower C14Ac concentration of 0.88 mM. In these experiments, the transitional pH was found to be ≈ 9 . The addition of glycerol to the solution was also found to affect significantly the transitional pH. For $C_{C14Ac} = 2.2$ mM, the addition of 40 wt% glycerol decreased the transitional pH from 10 to 9.

The obtained results for the dimensionless foam-wall stress are shown in Fig. 8B. The transitional pH for foam-wall friction (from immobile to mobile bubble surface) is again between 10 and 11, at 2.2 mM C14Ac.

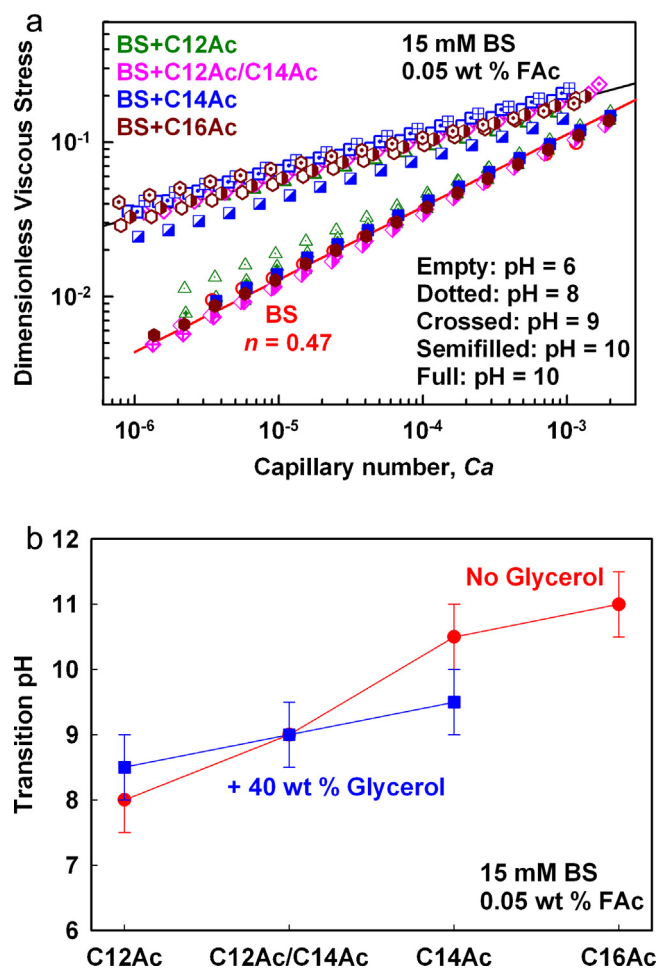


Fig. 9. (A) Dimensionless viscous stress, as a function of capillary number, for foams formed from BS (red circles); BS+C12Ac (green triangles); BS+C12Ac/C14Ac (pink diamonds); BS+C14Ac (blue squares) and BS+C16Ac (dark red hexagons) at pH = 6 (empty symbols); pH = 8 (dotted symbols); pH = 9 (crossed symbols); pH = 10 (semifilled symbols), and pH = 11 (full symbols). (B) Transitional pH, above which the foams formed from different BS+FAC solutions behave as foam formed from BS solution alone. (For interpretation of the references to colour in this figure legend, the reader is referred to the web version of this article.)

From these series of experiments we can conclude that the BS+C14Ac foams, formed at $C_{C14Ac} = 2.2$ mM and 0.88 mM, behave as with tangentially immobile bubble surfaces in foam rheology at $pH \leq 8$. The transition to mobile bubble surfaces depends significantly on C14Ac concentration and occurs at pH = 9 for 0.88 mM C14Ac and at pH between 10 and 11 for 2.2 mM C14Ac in the foaming solution.

3.3.3. Effects of FAC chain length and glycerol on foam rheological properties

In Fig. 9 we present results for the viscous friction in foams, stabilized with BS and different fatty acids, at pH varied between 6 and 11. At the lower pH values, we measure higher viscous friction and lower power-law index, $n < 0.3$. Upon increase of pH, the foam viscous stress sharply drops to the values for the BS system. The transition is observed at different pH values for the studied systems as follows: pH \approx 8 for BS+C12Ac, pH \approx 9 for BS+C12Ac+C14Ac, pH \approx 10.5 for C14Ac and pH \approx 11 for C16Ac-containing foams, see Fig. 9B. Thus we see that, at fixed total concentration of the fatty acid, the transitional pH is higher for systems containing fatty acids with longer chain lengths.

The transitional pH for C12Ac and C12Ac+C14Ac solutions is affected very slightly by the addition of glycerol. A decrease by

about 1 pH unit is observed in the transitional pH for BS+C14Ac solution, when glycerol is added, see Fig. 9B.

It is worth clarifying that at pH below the transitional one, viz. at high surface modulus of the solutions, no significant difference is detected for the dimensionless viscous stress in the various systems studied (different fatty acids and different pHs), see Fig. 9A. In other words, the different values of G_D , measured with the various fatty acids (Fig. 5B), do not change the foam viscous stress, when the latter is presented in dimensionless form.

4. Discussion

4.1. Surface properties

The obtained results show that a dense adsorption layer is formed on the bubble surface at high C14Ac concentrations and pH = 6, with equilibrium surface tension ≈ 22 mN/m (note that this is the typical value for the interfacial tension of aliphatic hydrocarbon-air interface [44]). In our previous study [26] we measured such low surface tension for BS+C14Ac solutions and explained it with the formation of surface condensed phase of C14Ac molecules in the adsorption layer. Such low surface tension was previously reported in literature for solutions of sodium myristate (no other surfactants) at pH \approx 8–9 [11,19]. According to literature [11], surface condensed phase of C14Ac molecules, giving such low surface tension, corresponds to surface density of $\approx 8 \times 10^{-6}$ mol/m², whereas the surface tension is much higher, ≈ 43 mN/m, when the surface density of C14Ac molecules is around two times lower, 4×10^{-6} mol/m².

Let us assume now that in our experiments, at $C_{C14Ac} \geq 0.44$ mM (where the surface modulus remains constant upon further increase of C_{C14Ac} , see Fig. 2B), dense adsorption layer of C14Ac molecules is formed on the bubble surface, corresponding to high surface modulus (≈ 380 mN/m), high viscous friction in the adsorption layer, and immobile bubble surfaces in foam-wall experiments (see Fig. 7). If we assume that the entire surface of the bubbles in the respective foam is covered by C14Ac molecules, we can estimate from a simple mass balance what minimal C14Ac concentration in the foaming solution would be sufficient to cover the bubble surface. Assuming that the total amount of C14Ac is adsorbed on the bubble surface, we can calculate the required C14Ac concentration from the formula [45,46]:

$$\Delta C = \frac{3\Phi\Gamma}{(1-\Phi)R_{32}} \quad (7)$$

Here Γ is C14Ac adsorption, Φ is air volume fraction in the foam (0.9 in our experiments), and R_{32} is the mean volume-surface radius. At $C_{C14Ac} \geq 0.44$ mM, the mean bubble radius remains almost constant, $R_{32} \approx 150$ μ m (see Fig. 6A). Using this value of R_{32} and $\Gamma_{C14Ac} = 8 \times 10^{-6}$ mol/m², we can estimate that the minimal concentration of C14Ac, needed to cover the entire bubble surface in these foams is 1.44 mM. In other words, the available C14Ac molecules in solutions with $C_{C14Ac} = 0.44$ mM are sufficient to cover only $\approx 30\%$ of the bubble surface. Therefore, we have to conclude that the remaining bubble surface is covered by SLES and CAPB molecules (the main surfactants in the used mixture). These estimates prove that a mixed adsorption layer of the main surfactants (SLES and CAPB) with C14Ac is formed on the bubble surfaces to provide high surface modulus and all other peculiar properties of these triple surfactant systems.

To check further the above conclusion, we calculated the C14Ac adsorption on the bubble surface for $C_{C14Ac} = 0.22$ mM, where the mean bubble radius is noticeably larger, $R_{32} \approx 240$ μ m, while the viscous friction in the surfactant adsorption layer is still high ($n < 0.3$) and the surface layers behave as immobile. Again assuming that all C14Ac molecules are adsorbed on the bubble surface,

we estimated that C14Ac adsorption is around 2×10^{-6} mol/m² (around 25% of the complete C14Ac monolayer) which is very close to the value estimated for the higher C14Ac concentrations. On the other hand, at $C_{C14Ac} = 0.11$ mM, where the mean bubble size is very similar, $R_{32} \approx 250$ μm, but the foams behave as stabilized by BS (no significant effect of C14Ac on foam properties), the estimated C14Ac adsorption is $\approx 10^{-6}$ mol/m², which is insufficient for rendering high surface modulus of the adsorption layer.

From all these estimates we conclude that the surface phase transition occurs when the surface concentration of the C14Ac molecules is in the range between 1×10^{-6} mol/m² and 2×10^{-6} mol/m².

To account for the possible redistribution of the C14Ac molecules between the surfactant micelles in the bulk solution and the adsorption layer, we used the experimental data for $\sigma(C_{C14Ac})$ shown in Fig. 1B. Because the concentration of the two basic surfactants (SLES and CAPB) is 15 mM, which is well above the CMC ≈ 0.5 mM, we can assume that the main effect of the added C14Ac molecules is to change the chemical potential of the surfactant molecules incorporated in the BS micelles (in other words, we consider the BS micelles as pseudo-phase, in which the C14Ac molecules are dissolved).

If we assume that the main surfactant molecules in the BS micelles are characterized by a chemical potential μ_1 (for simplicity, we use μ_1 as the average chemical potential of SLES and CAPB molecules in the solution in the following consideration), while C14Ac molecules are characterized by a chemical potential, μ_2 , the Gibbs–Duhem relation for the mixture BS + C14Ac requires:

$$N_1 d\mu_1 + N_2 d\mu_2 = 0 \quad (8)$$

Here N_1 is the number of BS molecules and N_2 is the number of C14Ac molecules incorporated in the micelles. For fixed volume of the surfactant solution, the above equation can be represented as:

$$C_1 d\mu_1 + C_2 d\mu_2 = 0 \quad (9)$$

where $C_1 = 15$ mM in our experiments and C_2 is the varied C14Ac concentration, as shown in Fig. 1B. For the change of the surface tension of these solutions, upon variation of C14Ac concentration, we can apply the Gibbs adsorption isotherm:

$$\Gamma_1 d\mu_1 + \Gamma_2 d\mu_2 = -d\sigma \quad (10)$$

where Γ_1 and Γ_2 are the adsorptions of the main surfactant and C14Ac, respectively. From Eq. (9) we can determine $d\mu_1$ as a function of $d\mu_2$. Assuming for ideal solution $d\mu_2 \approx RT d \ln C_2$, we derive the following approximate expression:

$$-\frac{d\sigma}{RT} = \left(\Gamma_2 - \Gamma_1 \frac{C_2}{C_1} \right) d \ln C_2 \quad (11)$$

where RT is the thermal energy. From Fig. 1B we see that the slope $d\sigma/d \ln C_2$ is virtually constant for C_{C14Ac} between 0.055 mM and 1.1 mM, and from this slope we can estimate $\Gamma_2 = \Gamma_{C14Ac}$ under the additional assumption that $\Gamma_1 C_2 / C_1 \ll \Gamma_2 \approx 4 \times 10^{-6}$ mol/m². Under these assumptions we estimated $\Gamma_2 / \Gamma_1 \equiv \Gamma_{C14Ac} / \Gamma_{BS} \approx 25\%$ in this range of C14Ac concentrations, which is in a very good agreement with the estimates described above, based on the mass balance of adsorbed C14Ac molecules. Besides, with these values of Γ_{C14Ac} and Γ_1 we can check *a posteriori* that the assumption $\Gamma_1 C_2 / C_1 \approx 0.02 \Gamma_2 \ll \Gamma_2$ is satisfied, indeed.

Thus we conclude that the adsorption layers in the triple systems with high surface modulus probably contain ≈ 70 – 75 molar% of the main surfactant molecules (CAPB and SLES) and ≈ 30 – 25 molar% of C14Ac molecules. The possible structure of such an adsorption layer is schematically shown in Fig. 10B. According to the proposed structure, the C14Ac molecules adsorb between the CAPB and SLES molecules in the adsorption layer and, thus,

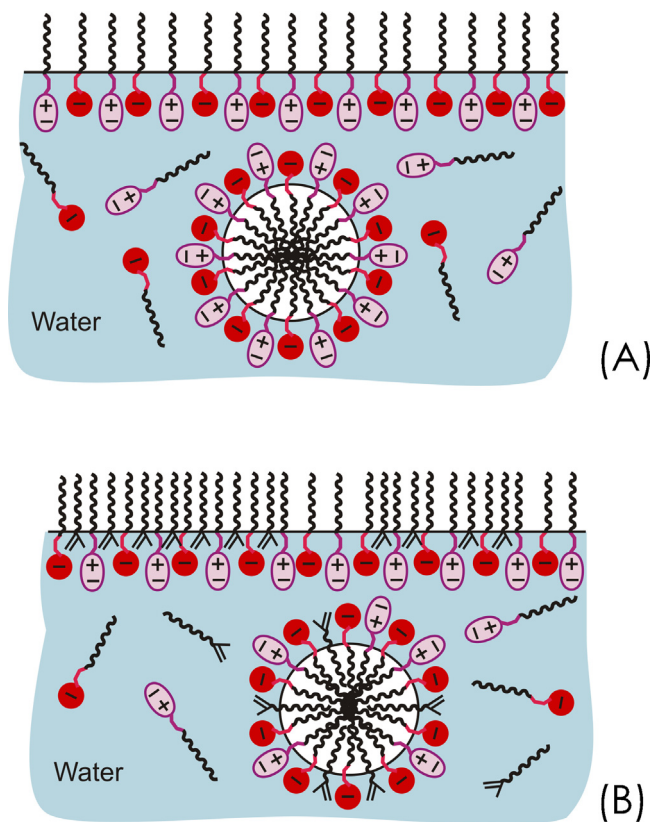


Fig. 10. Schematic presentation of the structure of adsorption layer: (A) In the absence of fatty acids, (B) In the presence of long-chain fatty acids (e.g., SLES + CAPB + C14Ac). The incorporation of FAC molecules in between the molecules of SLES and CAPB in the adsorption layer, induces a surface phase transition and formation of surface condensed phase.

decrease significantly the average area per surfactant molecule in the adsorption layer.

Based on the proposed structure of the adsorption layer, let us explain now the observed dependences of the surface properties of BS + C14Ac solutions on pH. The experimental fact that the mixed BS + C14Ac systems have very similar properties at pH = 3 and pH = 6 is a clear indication that the main entities, which co-adsorb with SLES and CAPB in this pH range, are non-ionized C14Ac molecules. Otherwise, we should expect very significant effect of pH on the solution surface properties, due to the variations in the ratio of ionized and non-ionized C14Ac molecules upon pH variation.

The increase of pH above the effective pK_a of C14Ac molecules, which is known [21,22] to be in the range 8.1–8.8, leads to a noticeable decrease of the concentration of non-ionized C14Ac molecules in the solution, which in turn explains the longer lag-time (Fig. 3A) and the lower surface modulus (Fig. 4A) at pH > 9. The most probable explanation for the longer lag-time is the decreased probability for formation of domains of surface condensed phase (due to the decreased concentration of non-ionized molecules in the adsorption layer). Note that the main fraction of C14Ac molecules is in ionized form at pH ≥ 9 , however, the myristic ions are not expected to co-adsorb between the molecules of the main surfactants (as the nonionic molecules of myristic acid do), due to the significant electrostatic repulsion between the negatively charged COO^- groups of the ionized C14Ac molecules and the negative charge of the adsorbed SLES molecules.

Interestingly, at pH = 9, after the formation of surface condensed phase in the adsorption layer, the measured surface moduli are very close to those measured at pH = 3, 6 and 8, which indicates that the structure of the condensed adsorption layer is conserved in a very

wide pH range, up to pH = 9. This result implies that the condensed adsorption layer should contain myristic acid (not sodium myristate molecules or myristate ions), because otherwise one should expect the layer properties to change with the increase of pH. In contrast, at pH = 10 the surface modulus remains noticeably lower after the observed phase transition (see Fig. 4), than the modulus measured at pH \leq 9. This difference indicates that the low concentration of non-ionized C14Ac molecules at pH = 10 (estimated as \approx 0.052 mM for $pK_a = 8.8$) leads to a different structure of the adsorption layer, with less C14Ac molecules incorporated – note that similar properties of the adsorption layer are observed at lower C14Ac concentration ($C_{C14Ac} = 0.055$ mM) and pH = 6.

The experimental data for the effect of fatty acid chain-length on the surface modulus, presented in Fig. 5B, could be explained with the increased chain order in the adsorption layer at longer chain-lengths, as reported in Refs. [1–6]. It should be mentioned that the studied basic surfactants, SLES and CAPB, contain subcomponents with different chain-lengths (coming from the production method of these surfactants of technical grade). As discussed by Tzocheva et al. [47], the surface properties of the SLES and CAPB solutions behave as being dominated by the chain-lengths of C16, which could be explained with the higher surface activity (and hence, the enhanced adsorption) of the subcomponents with longer chain lengths in the mixture.

4.2. Foam rheology

The experiments, performed at different C14Ac concentrations, shown in Fig. 7, clearly demonstrate that the transition between the two rheological regimes (with low and high surface modulus, respectively) occurs between 0.11 mM and 0.22 mM C14Ac in the foaming solutions. The measured surface modulus at $C_{C14Ac} = 0.11$ mM are below 100 mN/m, whereas those measured at $C_{C14Ac} = 0.22$ mM are higher than 100 mN/m, see Fig. 2.

On the other hand, the experiments performed with BS + C14Ac at different pH values showed this transition to occur around pH = 10, see Fig. 8. It should be mentioned that at pH = 10 we measure $G_D \approx 3$ mN/m for not aged adsorption layers, which should result in foam viscous stress similar to that of the BS solution. This apparent discrepancy of the results obtained by the foam rheology measurements (showing behavior of HSM system) and oscillating drop measurements (showing LSM system) is easily explained by the observed significant increase of the surface modulus after sufficient aging of the adsorption layer for this system, see Fig. 4B. Because the hydrodynamics during foaming is more forceful than that during measuring the surface modulus, we can expect much faster formation of surface condensed phase on the bubble surfaces during foaming (due to intensive convective flows in the sheared foam), as compared to the oscillating drop experiments. As a consequence, the surface modulus of the bubbles in BS + C14Ac stabilized foams, at pH = 10, seem to have high surface modulus, just as observed in the ODM method after long surface aging. This explanation is supported also by the observation that the total shear stress for this system, as measured in consecutive runs with foams in the rheometer, increased in the first several runs at pH = 10, whereas no such “foam aging” was observed at pH = 6 and pH = 11, see Fig. S5 in Supporting information.

From all accumulated experimental results we can conclude that the threshold value of G_D to observe a switch in the regime of foam viscous friction from LSM to HSM regime is $G_D \approx 100$ mN/m. Also, all foams with HSM > 100 mN/m behaved as with immobile bubble surfaces in the foam-wall experiments. This means that the threshold value for surface immobilization is around \approx 100 mN/m (for viscosity of the foaming solutions \approx 1 mPa s).

One important question which has emerged from these experimental results (from the mechanistic viewpoint) is why the

dimensionless surface dissipation in the foams, formed from solutions with different surface moduli (spanning the range between 100 mN/m and 400 mN/m), all fall around the same master line, without noticeable dependence of the dimensionless foam viscous stress on the specific value of the surface modulus. According to the theoretical analysis presented in our previous study [37], the viscous dissipation should increase with the increase of surface modulus, if the relative deformation of the bubble surface area is the same in all systems (at given foam shear rate). However, we observed in the oscillating drop method that the systems with higher surface modulus resisted very significantly the surface deformation – the measured amplitude of surface deformation was significantly smaller at higher surface modulus (under otherwise equivalent conditions). The latter result indicates that the relative surface deformation of the bubbles in sheared foams could be different for foams with high and low surface moduli (at the same shear rate). Therefore, more detailed rheological models should be developed to describe quantitatively the rheological properties of the systems with high surface modulus.

5. Conclusions

We performed a systematic experimental study of the effects of several factors on the surface tension, surface dilatational modulus, viscous friction inside sheared foam, foam-wall friction, and mean bubble size in sheared foams, for triple surfactant mixtures containing SLES, CAPB and long-chain fatty acids.

The obtained main results and conclusions could be summarized as follows:

- When varying the concentration of Myristic acid (C14Ac) in the mixture, C_{C14Ac} , we observed two ranges: At $C_{C14Ac} < 0.06$ mM, the acid increases solution surface modulus up to 50 mN/m, however, without affecting significantly any of the other properties studied. At $C_{C14Ac} > 0.11$ mM, C14Ac leads to significant decrease of surface tension (from 29 to 22 mN/m), increase of surface modulus (from 50 to 400 mN/m), decrease of mean bubble size in sheared foams (from 300 to 150 μ m), and strong increase of the inside-foam friction and foam-wall friction.
- For all systems studied, the increase of pH above a certain transitional value leads to a sharp increase of surface tension and decrease of surface dilatational modulus, which is accompanied with a decrease in the inside-foam and foam-wall viscous friction. The transitional pH value varies between 8 and 11, and increases with the fatty acid chain-length.
- The main effect of glycerol is to decrease the transitional pH (by 1 to 1.5 units for 40 wt% glycerol), without affecting significantly the system properties away from the transitional pH.
- The main role of C14Ac in these triple mixtures is to induce a surface phase transition, leading to formation of surface condensed phase in the adsorption layer. This transition occurs when the molar fraction of C14Ac in the mixed adsorption layer approaches ca. 30%. The surface condensed phase has low surface tension (below 26 mN/m) and high surface modulus (HSM).
- When the surface modulus of the foaming solutions increases above ca. 100 mN/m, we observe a sharp, step-wise change in the rheological properties of the foams and related decrease in the mean bubble size in sheared foams.
- Interestingly, the results for foam rheological properties of all HSM systems are very similar, when presented in dimensionless form, despite the fact that the surface modulus had been varied in a wide range (from ca. 100 to 400 mN/m).

The molecular mechanisms, relating the surface modulus of the foaming solutions with the foam rheological properties are still a

matter of intensive debate in literature [48–51]. The experimental results, obtained in the current study, could serve as useful tests for the theoretical models, trying to explain the role of surface properties on foam rheological properties.

Acknowledgments

The authors are grateful to Mrs. Mila Temelska and Ms. Julieta Popova for the measurements of surface modulus (both from Sofia University). The study is supported by Unilever R&D Center in Trumbull, USA, and by the FP7 European project “Beyond Everest”.

Appendix A. Supplementary data

Supplementary data associated with this article can be found, in the online version, at <http://dx.doi.org/10.1016/j.plantsci.2004.08.011>.

References

- [1] E.D. Goddard, O. Kao, H.C. Kung, Monolayer properties of fatty acids: IV. Influence of cation at high pH, *J. Colloid Interface Sci.* 24 (1967) 297.
- [2] H. Hasmonay, A. Hochapfel, P. Peretti, Equilibrium position of carboxylic acid molecules in monolayers on aqueous subphases, *J. Colloid Interface Sci.* 149 (1992) 247.
- [3] J. Daillant, L. Bosio, J.J. Benattar, C. Blot, Interaction of cations with a fatty acid monolayer. A grazing incidence x-ray fluorescence and reflectivity study, *Langmuir* 7 (1991) 611.
- [4] A. Gericke, H. Hühnerfuss, In situ investigation of saturated long-chain fatty acids at the air/water interface by external infrared reflection-absorption spectrometry, *J. Phys. Chem.* 97 (1993) 12899.
- [5] A. Gericke, H. Hühnerfuss, The effect of cations on the order of saturated fatty acid monolayers at the air-water interface as determined by infrared reflection-absorption spectrometry, *Thin Solid Films* 245 (1994) 74.
- [6] A. Gericke, R. Mendelsohn, Partial chain deuteration as an IRRAS probe of conformational order of different regions in hexadecanoic acid monolayers at the air/water interface, *Langmuir* 12 (1996) 758.
- [7] J. Simon-Kutscher, A. Gericke, H. Hühnerfuss, Effect of bivalent Ba, Cu, Ni, and Zn cations on the structure of octadecanoic acid monolayers at the air-water interface as determined by external infrared reflection-absorption spectroscopy, *Langmuir* 12 (1996) 1027.
- [8] K.A. Coltharp, E.I. Franses, Equilibrium and dynamic surface tension behavior of aqueous soaps: Sodium octanoate and sodium dodecanoate (sodium laurate), *Colloids Surf. A* 108 (1996) 225.
- [9] C.H. Chang, K.A. Coltharp, S.Y. Park, E.I. Franses, Surface tension measurements with the pulsating bubble method, *Colloids Surf. A* 114 (1996) 185.
- [10] X. Wen, K.C. McGinnis, E.I. Franses, Unusually low dynamic surface tensions of aqueous solutions of sodium myristate, *Colloids Surf. A* 143 (1998) 371.
- [11] X. Wen, J. Lauterbach, E.I. Franses, Surface densities of adsorbed layers of aqueous sodium myristate inferred from surface tension and infrared reflection absorption spectroscopy, *Langmuir* 16 (2000) 6987.
- [12] X. Wen, E.I. Franses, Effect of protonation on the solution and phase behavior of aqueous sodium myristate, *J. Colloid Interface Sci.* 231 (2000) 42.
- [13] P. Tippmann-Krayer, H. Mohwald, Precise determination of tilt angles by x-ray diffraction and reflection with arachidic acid monolayers, *Langmuir* 16 (1991) 6987.
- [14] K.D. Wantke, H. Fruhner, J. Fang, K. Lunkenheimer, Measurements of the surface elasticity in medium frequency range using the oscillating bubble method, *J. Colloid Interface Sci.* 208 (1998) 34.
- [15] J.B. Gilman, T.L. Eliason, A. Fast, V. Vaida, Selectivity and stability of organic films at the air-aqueous interface, *J. Colloid Interface Sci.* 280 (2004) 234.
- [16] J. Fang, K.D. Wantke, K. Lunkenheimer, Rheological properties of fatty acid solutions at the air/water interface, *J. Colloid Interface Sci.* 182 (1996) 31.
- [17] O. Albrecht, H. Matsuda, K. Eguchi, T. Nakagiri, The dissolution of myristic acid monolayers in water, *Thin Solid Films* 338 (1999) 252.
- [18] K.D. Danov, P.A. Kralchevsky, K.P. Ananthapadmanabhan, A. Lips, Interpretation of surface-tension isotherms of n-alkanoic (fatty) acids by means of the van der Waals model, *J. Colloid Interface Sci.* 300 (2006) 809.
- [19] P.A. Kralchevsky, K.D. Danov, C.I. Pishmanova, S.D. Kralchevska, N.C. Christov, K.P. Ananthapadmanabhan, A. Lips, Effect of the precipitation of neutral-soap, acid-soap, and alkanolic acid crystallites on the bulk pH and surface tension of soap solutions, *Langmuir* 23 (2007) 3538.
- [20] J.G. Petrov, T. Pfohl, T. Molthwald, Ellipsometric chain length dependence of fatty acid langmuir monolayers. A heads-and-tails model, *J. Phys. Chem.* 103 (1999) 3417.
- [21] J.R. Kanicky, A.F. Poniatowski, N.R. Mehta, D.O. Shah, Cooperativity among molecules at interfaces in relation to various technological processes: effect of chain length on the pK_a of fatty acid salt solutions, *Langmuir* 16 (2000) 172.
- [22] J.R. Kanicky, D.O. Shah, Effect of premicellar aggregation on the pK_a of fatty acid soap solutions, *Langmuir* 19 (2003) 2034.
- [23] N.D. Denkov, V. Subramanian, D. Gurovich, A. Lips, Wall slip and viscous dissipation in sheared foams: effect of surface mobility, *Colloids Surf. A* 263 (2005) 129.
- [24] N.D. Denkov, S. Tcholakova, K. Golemanov, V. Subramanian, A. Lips, Foam-wall friction: effect of air volume fraction for tangentially immobile bubble surface, *Colloid Surf. A* 329 (2006) 282–283.
- [25] K. Golemanov, S. Tcholakova, N.D. Denkov, K.P. Ananthapadmanabhan, A. Lips, Breakup of bubbles and drops in steadily sheared foams and concentrated emulsions, *Phys. Rev. E* 78 (2008) 051405.
- [26] K. Golemanov, N.D. Denkov, S. Tcholakova, M. Vethamuthu, A. Lips, Surfactant mixtures for control of bubble surface mobility in foam studies, *Langmuir* 24 (2008) 9956.
- [27] N.D. Denkov, S. Tcholakova, K. Golemanov, K.P. Ananthapadmanabhan, A. Lips, The role of surfactant type and bubble surface mobility in foam rheology, *Soft Matter* 5 (2009) 3389.
- [28] S. Tcholakova, Z. Mitrinova, K. Golemanov, N.D. Denkov, M. Vethamuthu, K.P. Ananthapadmanabhan, Control of Ostwald ripening by using surfactants with high surface modulus, *Langmuir* 27 (2011) 14807.
- [29] S. Dorbolo, D. Terwagne, R. Delhalle, J. Dujardin, N. Huet, N. Vandewalle, N. Denkov, Antibubble lifetime: influence of the bulk viscosity and of the surface modulus of the mixture, *Colloid Surf. A* 365 (2010) 43.
- [30] N. Adami, S. Dorbolo, H. Caps, Single thermal plume in locally heated vertical soap films, *Phys. Rev. E* 84 (2011) 046316.
- [31] A.L. Biance, A. Delbos, O. Pitois, How topological rearrangements and liquid fraction control liquid foam stability, *Phys. Rev. Lett* 106 (2011) 068301.
- [32] B. Dollet, Local description of the two-dimensional flow of foam through a contraction, *J. Rheology* 54 (2010) 741.
- [33] J. Emile, A. Salonen, B. Dollet, A. Saint-Jalmes, A systematic and quantitative study of the link between foam slipping and interfacial viscoelasticity, *Langmuir* 25 (2009) 13412.
- [34] A.L. Biance, S. Cohen-Addad, R. Höhler, Topological transition dynamics in a strained bubble cluster, *Soft Matter* 5 (2009) 4672.
- [35] P.R. Garrett, J.D. Hines, S.C. Joyce, P.T. Whittall, Report prepared for Unilever R&D, Port Sunlight, 1993.
- [36] S. Mukherjee, H. Wiedersich, Morphological and viscoelastic properties of dense foams generated from skin cleansing bars, *Colloids Surf.* 95 (1995) 159.
- [37] S. Tcholakova, N.D. Denkov, K. Golemanov, K.P. Ananthapadmanabhan, A. Lips, Theoretical model of viscous friction inside steadily sheared foams and concentrated emulsions, *Phys. Rev. E* 78 (2008) 011405.
- [38] H.M. Princen, The structure, mechanics, and rheology of concentrated emulsions and fluid foams, in: J. Sjöblom (Ed.), *Encyclopedia of Emulsion Technology*, Marcel Dekker, New York, 2001, p. 243, ch. 11.
- [39] D. Weaire, The rheology of foam, *Curr. Opin. Colloid Interface Sci.* 13 (2008) 171.
- [40] A.M. Kraynik, Foam flows, *Ann. Rev. Fluid Mech.* 20 (1988) 325.
- [41] H.M. Princen, Rheology of foams and highly concentrated emulsions: I. Elastic properties and yield stress of a cylindrical model system, *J. Colloid Interface Sci.* 91 (1983) 160.
- [42] H.M. Princen, Rheology of foams and highly concentrated emulsions. II. Experimental study of the yield stress and wall effects for concentrated oil-in-water emulsions, *J. Colloid Interface Sci.* 105 (1985) 150.
- [43] H.M. Princen, A.D. Kiss, Rheology of foams and highly concentrated emulsions: IV. An experimental study of the shear viscosity and yield stress of concentrated emulsions, *J. Colloid Interface Sci.* 128 (1989) 176.
- [44] J.N. Israelachvili, in: *Intermolecular and Surface Forces*, Second ed., Academic Press, New York, 1992.
- [45] S. Tcholakova, N.D. Denkov, D. Sidzhakova, I.B. Ivanov, B. Campbell, Interrelation between drop size and protein adsorption at various emulsification conditions, *Langmuir* 19 (2003) 5640.
- [46] S. Tcholakova, N.D. Denkov, T. Danner, Role of surfactant type and concentration for the mean drop size during emulsification in turbulent flow, *Langmuir* 20 (2004) 7444.
- [47] S.S. Tzocheva, P.A. Kralchevsky, K.D. Danov, G.S. Georgieva, A.J. Post, K.P. Ananthapadmanabhan, Solubility limits and phase diagrams for fatty acids in anionic (SLES) and zwitterionic (CAPB) micellar surfactant solutions, *J. Colloid Interface Sci.* 369 (2012) 274.
- [48] M.B. Sexton, M.E. Möbius, S. Hutzler, Bubble dynamics and rheology in sheared two-dimensional foams, *Soft Matter* 7 (2011) 11252.
- [49] J.R. Seth, L. Mohan, C. Locatelli-Champagne, M. Cloitre, R.T. Bonnecaze, A micromechanical model to predict the flow of soft particle glasses, *Nat. Mater.* 10 (2011) 838.
- [50] I. Cantat, Gibbs elasticity effect in foam shear flows: a non quasi-static 2D numerical simulation, *Soft Matter* 7 (2011) 448.
- [51] D. Weaire, J.D. Barry, S. Hutzler, The continuum theory of shear localization in two-dimensional foam, *J. Phys. Condens. Matter* 22 (2010) 193101.